

Supplementary material for “Coherent Josephson qubit suitable for scalable quantum integrated circuits”

R. Barends,^{1,*} J. Kelly,^{1,*} A. Megrant,¹ D. Sank,¹ E. Jeffrey,¹ Y. Chen,¹ Y. Yin,^{1,†} B. Chiaro,¹ J. Mutus,¹ C. Neill,¹ P. O’Malley,¹ P. Roushan,¹ J. Wenner,¹ T. C. White,¹ A. N. Cleland,¹ and John M. Martinis¹

¹*Department of Physics, University of California, Santa Barbara, CA 93106, USA*

DEVICE FABRICATION

The devices were made in a two-step deposition process. The qubit capacitor, groundplane, readout resonator and control and readout wiring were made in a first, separate deposition step. We used molecular beam epitaxy (MBE) Al deposited on a *c*-plane sapphire substrate. The Al film thickness is approximately 100 nm, deposited at room temperature. The sapphire substrate was cleaned by load-lock outgassing at 200 °C, followed by heating to 850 °C in $\sim 10^{-6}$ Torr activated oxygen, identical to the process outlined in Ref. [1]. The first Al layer was patterned by a BCl_3/Cl_2 reactive ion etch.

In the final step, $0.30 \times 0.20 \mu\text{m}^2$ Al tunnel barriers (30 nm bottom and 100 nm top layer thickness) were made using double-angle shadow evaporation. We used

a high vacuum electron-beam evaporator, with a base pressure of approximately 5×10^{-8} Torr. We used the Dolan bridge technique with a poly(methyl methacrylate)/copolymer resist bilayer (approximate thickness: 0.30 and 0.50 μm , respectively), patterned with electron beam lithography. In order to make galvanic contact between the first Al layer and the junction layer, we used a 3 min long Ar ion mill (beam: 400 V, 21 mA; beam width: $\sim 3.2''$) before shadow-evaporation. Approximately 40 nm was removed from the top resist layer during the ion mill. The junctions were oxidized for 80 mins at 5.0 mBar. Lift-off was done in N-methyl-2-pyrrolidinone at 80 °C.

We find that the junctions age very little, the resistance value changes less than 1% over a period of ten days. An optical micrograph of the devices is shown in Fig. S1.

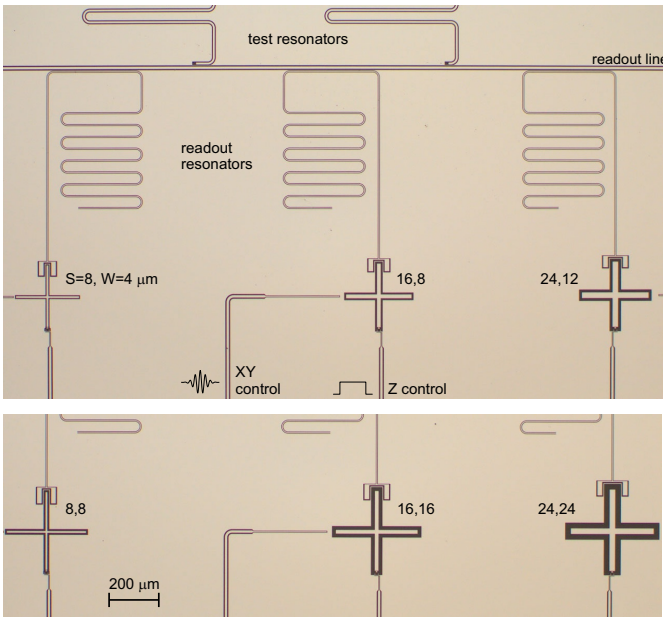


FIG. S1: (Color online) Optical micrograph of the six ‘Xmon’ qubits on two chips, formed by the Al superconducting (light) and the exposed sapphire substrate (dark). The qubits are capacitively coupled to readout resonators, which couple to a readout line in a frequency multiplexed readout scheme [2]. The central linewidth S and gap width W are varied from 8,4 μm to 24,24 μm . The top three Xmons have a single arm length of $L = 130 \mu\text{m}$, the bottom three have $L = 165 \mu\text{m}$. Test resonators provide an independent measurement of the quality factor.

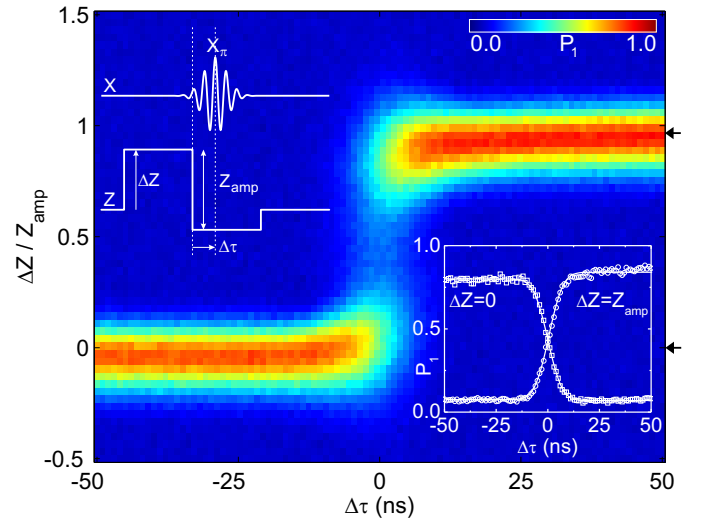


FIG. S2: (Color online) Z pulse shape measurement. The qubit is excited with a π -pulse with 20 ns Gaussian envelope, while a rectangular wave is applied on the Z line. The pulse sequence is shown in the left inset. We use $Z_{\text{amp}} = 0.2$ (arb. units) [3], which corresponds to a shift in frequency of 73 MHz. The right inset is a cross section at $\Delta Z = 0$ (squares) and $\Delta Z = Z_{\text{amp}}$ (circles), as indicated by the arrows (right). The solid lines are fits to partial qubit rotations from a π -pulse with a truncated Gaussian envelope.

Z PULSE

In order to quantify the response time of the qubit to a Z pulse, we simultaneously apply a π -pulse with a Gaussian envelope on the XY control and a rectangular wave pattern on the Z control line. The pulse sequence is shown in the left inset in Fig. S2. We slide the rectangular wave in time ($\Delta\tau$) and offset (ΔZ), while retaining the amplitude of the wave Z_{amp} constant. The excited state population is plotted in Fig. S2 as a function of time and amplitude.

A cross section of the main figure at $\Delta Z = 0$ (squares) and $\Delta Z = Z_{\text{amp}}$ (circles) is shown in the right inset. The measured response can be accurately described by qubit rotation from a partial π -pulse (π -pulse duration: 20 ns), with a truncated Gaussian as envelope (solid lines): with the quantum state given by $\Psi = \cos(\frac{\theta}{2})|0\rangle + \sin(\frac{\theta}{2})|1\rangle$, for the fall at $\Delta Z = 0$: $\theta = \int_{-\infty}^{-\Delta\tau} \sqrt{\pi/2} \exp[-t^2/2\sigma^2]/\sigma dt$. No other time constants are included. We find that the rise at $\Delta Z = Z_{\text{amp}}$ is best described when assuming a 0.5 ns delay compared to the fall at $\Delta Z = 0$. We conclude that the qubit frequency is tuned to the desired frequency on a timescale of nanoseconds.

We find the Z control cross-talk between adjacent Xmons to be 1.0-1.5%.

QUBIT DECAY RATE

The frequency-dependent decay rate is displayed in Fig. S3, replotted from the data in Fig. 4 in the main text.

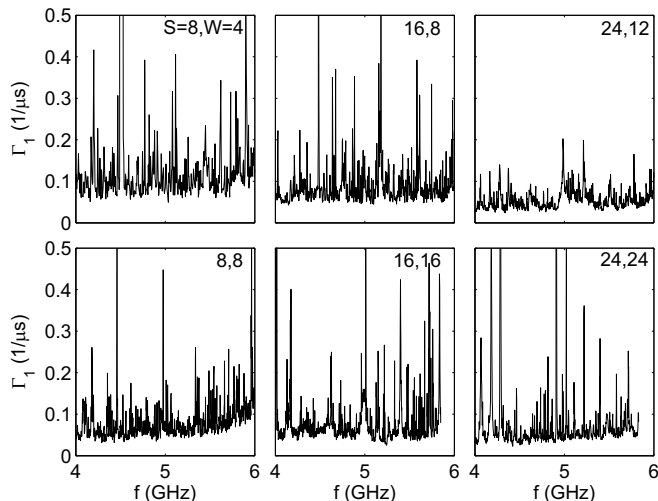


FIG. S3: Frequency dependence of Γ_1 for six qubits with different S and W . The frequency stepsize is 5 MHz for $S, W = 8, 4 \mu\text{m}$ and 2 MHz otherwise.

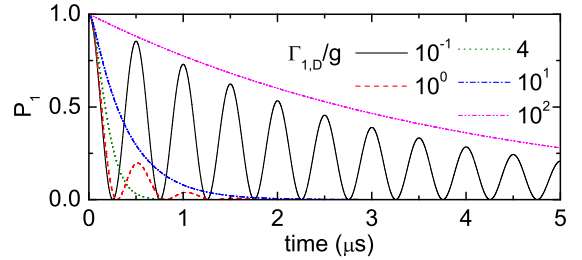


FIG. S4: (Color online) Qubit excited state probability versus time, in a simulation of a qubit-defect system. The qubit is on resonance with the defect, whose energy relaxation time is $\Gamma_{1,D}$. Here, we used a coupling strength $g/2\pi = 1$ MHz.

SIMULATION OF A QUBIT-DEFECT SYSTEM

In order to elucidate coherent as well as incoherent decay of the qubit state, we numerically simulate a qubit-defect system. The system consists of two coupled two-level systems, with coupling strength g and defect energy decay rate $\Gamma_{1,D}$; the qubit is placed on resonance with the defect. The qubit excited state probability is shown in Fig. S4. For $\Gamma_{1,D} < 4g$, the excitation coherently swaps back and forth between qubit and defect, decaying slowly. When the decay rate exceeds the coupling strength ($\Gamma_{1,D} > 4g$) coherent swapping vanishes and an exponential decay appears, as the qubit state decays incoherently. The excitation decays most quickly for $\Gamma_{1,D} = 4g$.

ANALYTICAL EXPRESSION FOR LOSS IN A QUBIT-DEFECT SYSTEM

Here we derive an analytical expression for the energy loss rate arising from a qubit coupling to a single two-level defect. We consider a system with two coupled two-level systems. We solve the master equation in the Lindblad form,

$$\dot{\rho} = -\frac{i}{\hbar}[H, \rho] + \sum_i \mathcal{D}[C_i] \rho, \quad (\text{S1})$$

with $\mathcal{D}[C] \rho = C\rho C^\dagger - (C^\dagger C\rho + \rho C^\dagger C)/2$ and the Hamiltonian given by

$$H = \hbar\omega_Q a^\dagger a + \hbar\omega_D b^\dagger b + \hbar g(b^\dagger \otimes a + b \otimes a^\dagger), \quad (\text{S2})$$

with a and b the lowering operator for qubit and defect, respectively, and ω the angular transition frequency. We model Markovian decoherence through the Lindblad terms: $C_{i=1-4} = \{a\sqrt{\Gamma_{1,Q}}, a^\dagger a\sqrt{2\Gamma_{\phi,Q}}, b\sqrt{\Gamma_{1,D}}, b^\dagger b\sqrt{2\Gamma_{\phi,D}}\}$, denoting

energy and phase relaxation for qubit and defect, respectively. Here we used the number operators a^+a and b^+b to express pure dephasing, and $\Gamma_{1,Q}$ denotes qubit relaxation. We take $\Gamma_{1,Q} \ll \Gamma_{1,D}$. As we are interested in the relaxation of a single excitation, we only consider the states $\{|00\rangle, |01\rangle, |10\rangle\}$. In the interaction picture and matrix form the above becomes

$$H = \hbar \begin{pmatrix} 0 & 0 & 0 \\ 0 & 0 & g \\ 0 & g & \Delta \end{pmatrix}, \quad (\text{S3})$$

$$\begin{aligned} \dot{\rho} = & -\frac{i}{\hbar}[H, \rho] \\ & -\frac{\Gamma_{1,Q}}{2} \begin{pmatrix} -2\rho_{22} & \rho_{12} & 0 \\ \rho_{21} & 2\rho_{22} & \rho_{23} \\ 0 & \rho_{32} & 0 \end{pmatrix} - \Gamma_{\phi,Q} \begin{pmatrix} 0 & \rho_{12} & 0 \\ \rho_{21} & 0 & \rho_{23} \\ 0 & \rho_{32} & 0 \end{pmatrix} \\ & -\frac{\Gamma_{1,D}}{2} \begin{pmatrix} -2\rho_{33} & 0 & \rho_{13} \\ 0 & 0 & \rho_{23} \\ \rho_{31} & \rho_{32} & 2\rho_{33} \end{pmatrix} - \Gamma_{\phi,D} \begin{pmatrix} 0 & 0 & \rho_{13} \\ 0 & 0 & \rho_{23} \\ \rho_{31} & \rho_{32} & 0 \end{pmatrix}, \end{aligned} \quad (\text{S4})$$

with ρ the density matrix, and $\Delta = \omega_D - \omega_Q$.

We are interested in the decay of the qubit excited state probability ρ_{22} , the relevant equations extracted from above are

$$\dot{\rho}_{22} = -ig(\overline{\rho_{23}} - \rho_{23}) - \Gamma_{1,Q}\rho_{22} \quad (\text{S5a})$$

$$\dot{\rho}_{23} = -ig(\rho_{33} - \rho_{22}) + i\Delta\rho_{23} - \Gamma\rho_{23} \quad (\text{S5b})$$

$$\dot{\rho}_{33} = -ig(\rho_{23} - \overline{\rho_{23}}) - \Gamma_{1,D}\rho_{33} \quad (\text{S5c})$$

with $\Gamma = \Gamma_{1,D}/2 + \Gamma_{\phi,D} + \Gamma_{1,Q}/2 + \Gamma_{\phi,Q}$.

In the limit $\Gamma_{1,D} > g$, $\rho_{33} \approx 0$, and we can approximate the system with two coupled differential equations. Inserting $\rho_{22} = \exp(-\Gamma_1 t)$ and $\rho_{23} = (\beta_r + i\beta_i) \exp(-\Gamma_1 t)$ gives

$$\Gamma_1 = 2g\beta_i + \Gamma_{1,Q} \quad (\text{S6a})$$

$$\Gamma_1\beta_r = \Delta\beta_i + \Gamma\beta_r \quad (\text{S6b})$$

$$\Gamma_1\beta_i = -g - \Delta\beta_r + \Gamma\beta_i, \quad (\text{S6c})$$

The solution for the qubit energy decay rate Γ_1 in the presence of a two-level defect is (for $\Gamma_{1,D} > g > \Gamma_{1,Q}$)

$$\Gamma_1 = \frac{2g^2\Gamma}{\Gamma^2 + \Delta^2} + \Gamma_{1,Q}. \quad (\text{S7})$$

We note that the above equation is similar to the low power limit of the two-level system response function, see for example Ref. [4].

MONTE CARLO SIMULATION OF DEFECTS IN THE XMON QUBIT

In order to quantitatively understand the Xmon qubit's energy decay as well as its variation over frequency, we have performed a Monte Carlo simulation

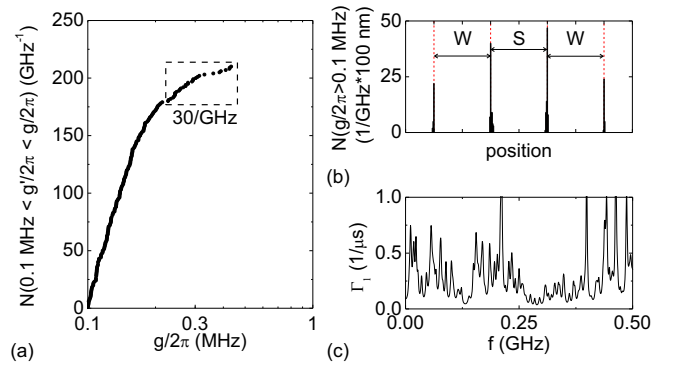


FIG. S5: (Color online) Monte Carlo simulation for defects in the Xmon capacitor, with $S=8$, $W=8 \mu\text{m}$ and the Xmon arm length $L=165 \mu\text{m}$. (a) Truncated cumulative distribution of the defect coupling strength. A total of 210 defects/GHz have a coupling strength $g/2\pi > 0.1$ MHz. A total of 30 defects/GHz have a coupling strength $g/2\pi > 0.22$ MHz. (b) Distribution of the defects along position; number of defects in each 100 nm wide section is plotted. The cross section of the capacitor is dashed. The coplanar waveguide geometry as well as the definition of S and W are shown in Fig. 1b in the main text. (c) The simulated decay rate in a 0.5 GHz bandwidth using the distribution in (a,b), and Eq. S7.

for defects in the capacitor. The defect density for AlO_x in tunnel barriers has been established in measurements with phase qubits [5], with the distribution over dipole moment p , volume, and frequency given by $\rho_0 \sqrt{1 - p^2/p_{\text{max}}^2}/p$, with $\rho_0 \approx 10^2/\mu\text{m}^3/\text{GHz}$, and the maximum dipole moment $p_{\text{max}} = 6 D$. As the capacitor metal oxide and exposed substrate both consist of Al oxide, we assume that these numbers are a fair representation of the defect density in the qubit capacitor. We only consider defects in the capacitor, the junction is assumed to contain no defects for this simulation.

We randomly place defects in a 3 nm thick dielectric layer ($\epsilon_r = 10$) on the substrate-air and metal-air interfaces (top metal surface as well as the etched edges). The substrate-metal interface is assumed to be thoroughly cleaned [1] and to contain no significant defect density. Using a thickness of 2 nm instead of 3 nm for the dielectric layer does not significantly influence the results. Each defect is given a random dipole moment p , such that the distribution over dipole moments matches: $\rho_0 \sqrt{1 - p^2/p_{\text{max}}^2}/p$, as given by Ref. [5]. The coupling strength $g = pE$ is then calculated for each defect using a simulation for the electric fields in our geometry. The results are shown in Fig. S5.

In Fig. S5a, we have plotted the truncated cumulative defect distribution over coupling strength. We find that, in a 1 GHz band, 30 defects have a coupling strength of $g/2\pi \gtrsim 0.2$ MHz (square). This simulated value is close to the experimentally observed density of $\sim 30/\text{GHz}$ in Fig. 3 in the main text. These strongly coupled defects are predominantly located within a ~ 100 nm dis-

tance from the etched metal edges, including the exposed substrate surface close to the metal edges and capacitor metal oxide, where the electric fields are largest, see Fig. S5b.

The simulated qubit decay rate for the same defect distribution is shown in Fig. S5c in a 0.5 GHz bandwidth. For the defect decay rate we have assumed, for defects with $g/2\pi > 0.1$ MHz, a uniform distribution based on the values extracted from Fig. 3 in the main text: $1/\Gamma_{2,D} = 50 - 100$ ns ($\Gamma_{2,D} = \Gamma_{1,D}/2 + \Gamma_{\phi,D}$). The simulated decay rate reproduces both the peaks as well as the variation in the background which are observed in the measurement.

* These authors contributed equally to this work

† Present address: Department of Physics, Zhejiang Univer-

- sity, Hangzhou 310027, China
- [1] A. Megrant, C. Neill, R. Barends, B. Chiaro, Y. Chen, L. Feigl, J. Kelly, E. Lucero, M. Mariantoni, P. J. J. O'Malley, D. Sank, A. Vainsencher, J. Wenner, T. C. White, Y. Yin, J. Zhao, C. J. Palmström, J. M. Martinis, A. N. Cleland, *Appl. Phys. Lett.* **100**, 113510 (2012).
 - [2] Y. Chen, D. Sank, P. O'Malley, T. White, R. Barends, B. Chiaro, J. Kelly, E. Lucero, M. Mariantoni, A. Megrant, C. Neill, A. Vainsencher, J. Wenner, Y. Yin, A. N. Cleland, J. M. Martinis, *Appl. Phys. Lett.* **101**, 182601 (2012).
 - [3] One Z unit corresponds to 0.5 mA in the control line on the chip.
 - [4] J. Gao, L. R. Vale, J. A. B. Mates, D. R. Schmidt, G. C. Hilton, K. D. Irwin, F. Mallet, M. A. Castellanos-Beltran, K. W. Lehnert, J. Zmuidzinas, and H. G. Leduc, *Appl. Phys. Lett.* **98**, 232508 (2011).
 - [5] J. M. Martinis, K. B. Cooper, R. McDermott, M. Steffen, M. Ansmann, K. Osborn, K. Cicak, S. Oh, D. P. Pappas, R. W. Simmonds, C. C. Yu, *Phys. Rev. Lett.* **95**, 210503 (2005).